CMS Physics Analysis Summary

Contact: cms-pag-conveners-exotica@cern.ch 2010/07/23

First Results on the Search for Stopped Gluinos in pp collisions at $\sqrt{s}$ = 7 TeV

The CMS Collaboration

Abstract

We present the first results of a search for long-lived gluinos which have stopped in the Compact Muon Solenoid (CMS) detector after being produced in 7 TeV pp collisions from CERN's Large Hadron Collider (LHC). We looked for the subsequent decay of these particles during time intervals where there were no pp collisions in the CMS experiment. In particular, we searched for decays during gaps between crossings in the LHC beam structure. We recorded such decays with a dedicated calorimeter trigger. In a dataset with a peak instantaneous luminosity of $1.3 \times 10^{30}\text{cm}^{-2}\text{s}^{-1}$, an integrated luminosity of 203 - 232 nb^{-1} depending on the gluino lifetime, and a search interval corresponding to 115 hours of LHC operation, no significant excess above background was observed. In the absence of a signal, we set a limit at 95% C.L. on gluino pair production over 14 orders of magnitude of gluino lifetime. This result extends existing limits from the Tevatron. For a mass difference $m_{\tilde{g}} - M_{\tilde{\chi}_1^0} > 100$ GeV, assuming BR($\tilde{g} \to g\tilde{\chi}_1^0$) = 100%, we are able to exclude lifetimes from 75 ns - 6 μs for $m_{\tilde{g}} = 200$ GeV/c^2. Furthermore we exclude gluino masses $m_{\tilde{g}} < 229$ GeV/c^2 with a lifetime of 200 ns using a time-profile analysis and $m_{\tilde{g}} < 225$ GeV/c^2 with a lifetime of 2.6 μs in a counting experiment.

1 Introduction

Many extensions to the Standard Model (SM) of particle physics predict the existence of new heavy quasi-stable charged particles [1]. Such particles are present in some supersymmetric models [2–4], "hidden valley" scenarios [5, 6], and grand unified theories (GUTs) where the new particles decay through GUT scale suppressed dimension 5 or 6 operators [7]. Long-lived particles are also a hallmark of split supersymmetry [8] where the gluino ($\tilde{g}$) decay is suppressed[1] due to the large gluino/squark mass splitting from which the theory gets its name. Of these possibilities, the Compact Muon Solenoid (CMS) experiment is most sensitive to models like split supersymmetry where production proceeds via the strong interaction with a (consequently) relatively large cross-section at the LHC [9–12]. As a result, we have targeted our search for long-lived gluinos. Existing experimental constraints on such a gluino's lifetime are weak [13]; they may well be stable on typical CMS experimental timescales. In particular, lifetimes $\mathcal{O}(100-1000)$ seconds are especially interesting in cosmology since such decays would affect the primordial light element abundances and could resolve the present discrepancy between the measured ^{6}Li, ^{7}Li abundances and conventional big bang nucleosynthesis [7, 14].

If long-lived gluinos are produced at CMS, they will hadronise into $\tilde{g}g, \tilde{g}q\bar{q}, \tilde{g}qqq$ states which are collectively known as "R-hadrons". In analogy with their mesonic and baryonic counterparts some of these gluino bound states will be charged whilst others will be neutral. Those which are charged will lose energy via ionisation as they traverse the CMS detector. For low-β R-hadrons, this energy loss is sufficient to bring a significant fraction of the produced particles to rest inside the CMS detector volume [15]. These "stopped" R-hadrons will decay seconds, days, or weeks later. These decays will be out-of-time with respect to LHC collisions and may well occur at times when there are no collisions (e.g. beam gaps) or when there is no beam in the LHC machine (e.g. interfill period). The observation of such decays, in what should be a quiet detector save for the occasional cosmic ray, would be an unambiguous discovery of new physics. This search is complementary to the search for heavy stable charged particles (HSCP) that track their passage through the CMS detector using energy loss and timing information [16] since it is sensitive to β less than ~ 0.3 for which these direct search techniques have negligible acceptance.

We have carried out the first such search using the strategy detailed in [17] with one notable difference. We have not yet searched in data collected during the interfill period between beam-dump and re-injection.

The data analyzed in this analysis summary were collected April-July 2010, at a centre-of-mass energy of 7 TeV. We divide the data into two samples; the first corresponds to 48 hours of trigger live-time during LHC fills, in which the instantaneous luminosity was $2-7\times10^{27}\mathrm{cm}^{-2}\mathrm{s}^{-1}$. We use this sample to estimate the background rate. There is no issue of signal contamination due to the low average instantaneous luminosity. The second sample, in which we search for the presence of a stopped particle signal, corresponds to 115 hours of trigger live-time, taken during fills for which the instantaneous luminosity averaged $6\times10^{29}\mathrm{cm}^{-2}\mathrm{s}^{-1}$, peaking at $1.3\times10^{30}\mathrm{cm}^{-2}\mathrm{s}^{-1}$. In both samples, we select events that fire a dedicated calorimeter jet trigger that also includes a "no-collision" condition. We then apply an offline selection designed to reject backgrounds due to beam effects, cosmic rays, and instrumental noise. Using the final rate estimated from the background sample, we perform a counting experiment in the search sample, as well as a shape analysis using the profile of observed event times. The LHC was sparsely filled with proton bunches in both the background and search datasets.

[1] We assume R-parity is conserved.

2 Signal Simulation

We have developed a custom simulation of gluino production, stopping and decay to determine our efficiency to this atypical signal. We factorize this simulation into 3 phases. In Phase 1, we generate gluino events at $\sqrt{s} = 7$ TeV using PYTHIA [18] to simulate the dominant leading order production processes, $q\bar{q} \to \tilde{g}\tilde{g}$ and $gg \to \tilde{g}\tilde{g}$. The lifetime of the gluino is set such that it is stable and we scan gluino masses from $m_{\tilde{g}} = 150 - 500$ GeV, a range for which the theoretical $\tilde{g}\tilde{g}$ production cross-section is sufficient that it can be probed with early LHC data. PYTHIA also hadronises the produced gluino into R-hadrons. GEANT4 [19] is used to simulate the interaction of these R-hadrons with the CMS detector. To accomplish this, GEANT4 employs the so-called "cloud model" for the interaction of stable heavy hadrons with matter [20]. Eventually, the R-hadron either stops in the material of the detector, or exits it. In the former case the coordinates of the stopping point and the flavour of the R-hadron are recorded.

Figure 1 shows the distribution of stopping points for $m_{\tilde{g}} = 200\,\mathrm{GeV}/c^2$. The material structure of the CMS detector is clearly seen in these distributions. Figure 2 presents the stopping probability as a function of gluino mass, obtained from the Phase 1 simulation. Nuclear interactions (NI) which depend on the cloud model introduce an uncertainty in the stopping probability. We therefore present the stopping probability from electromagnetic interactions (EM) alone, as well as that obtained from the combined effects of EM+NI. Some models [21] predict the lightest R-baryon ($\tilde{g}qqq$) state to be neutral, thus other R-baryons should quickly fall to this neutral state, and therefore escape the detector. In such models, only R-mesons ($\tilde{g}q\bar{q}$) will stop. Hence we also present the stopping probability for this "neutral R-baryon" case.

In Phase 2, we simulate the decay of the stopped R-hadron. Implicit in our factorisation approach is the assumption that this decay takes place at a time that is much greater than the time required to stop the R-hadron. Thus we use PYTHIA to produce an R-hadron (with its flavour record from Phase 1) at rest at $(0, 0, 0)$. Subsequently, we translate the R-hadron from this nominal vertex position to a randomly chosen stopping location determined in Phase 1 and decay it instantaneously.

The kinematics of a R-hadron decay is dominated by the properties of the gluino and neutralino - the spectator quarks do not play a significant role. These spectator quarks cannot be ignored, however, as they participate in hadronisation of the produced gluon or quarks. We developed and implemented a customized decay table to correctly describe these decays where a color-neutral R-baryon decays into a colored gluino, quark, and diquark with appropriate color structure. The gluino itself can decay into a neutralino and either a gluon or quark-antiquark pair:

$$\Delta_{\tilde{g}}^{++}[\tilde{g}\,u(uu)] \to g\,\tilde{\chi}_1^0\,u(uu)$$
$$\Delta_{\tilde{g}}^{++}[\tilde{g}\,u(uu)] \to q\bar{q}\,\tilde{\chi}_1^0\,u(uu)$$

Similarly a color-neutral R-meson can decay into a colored gluino, quark and antiquark, with the following gluino decay:

$$\rho_{\tilde{g}}^{+}[\tilde{g}\,u\bar{d}] \to g\,\tilde{\chi}_1^0\,u\bar{d}$$
$$\rho_{\tilde{g}}^{+}[\tilde{g}\,u\bar{d}] \to q\bar{q}\,\tilde{\chi}_1^0\,u\bar{d}$$

In the analysis presented in this PAS, we assume BR($\tilde{g} \to g\tilde{\chi}_1^0$) = 100% as in split supersymmetry. Finally, PYTHIA hadronises the decay products, and parton-showering proceeds as usual.

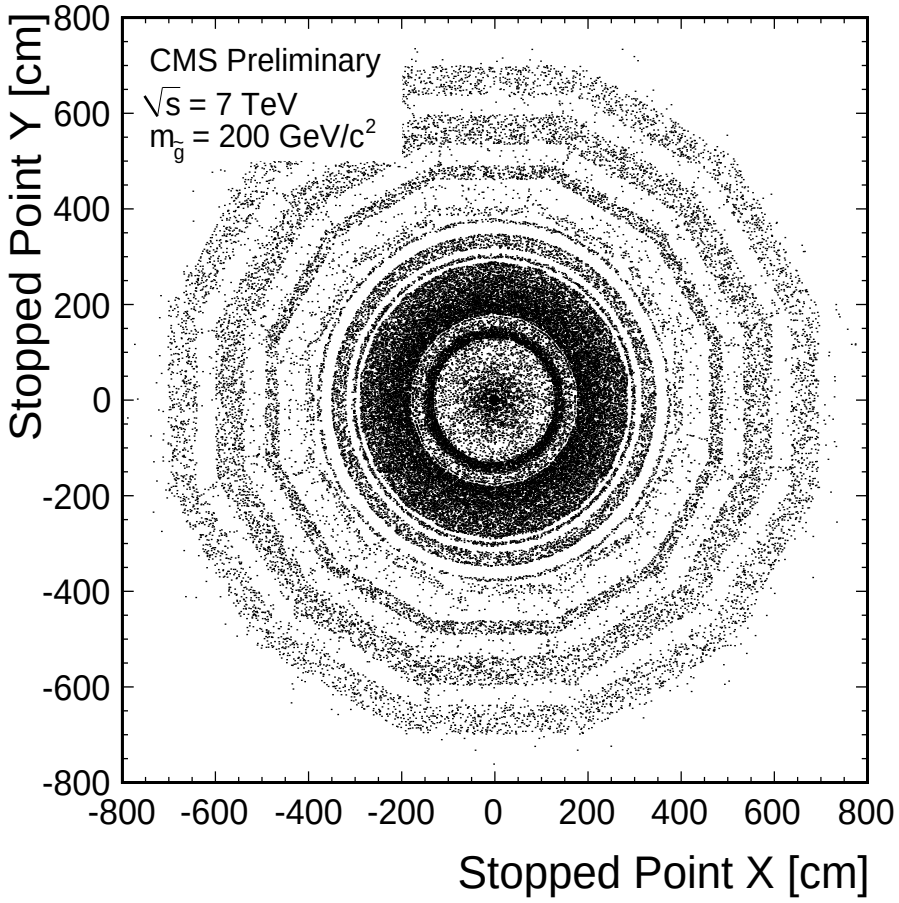

Figure 1: R-hadron stopping points for $m_{\tilde{g}} = 200$ GeV, and $\sqrt{s} = 7$ TeV.

These fully simulated stopped gluino events are passed on to trigger emulation, then to default reconstruction, and are finally analysed as normal Monte Carlo data. With Phase 2 of the simulation we are thus able to estimate trigger and reconstruction efficiencies for any set of online and offline cuts.

Phase 3 of our simulation uses a toy Monte Carlo to determine how often a stopped-gluino decay will occur during a beam gap. It takes as input the stopping efficiency determined in Phase 1 and the combined trigger times reconstruction efficiency obtained in Phase 2. These efficiencies are multiplied together and then multiplied by the production cross-section, to determine the total number of detectable decays per unit integrated luminosity. The record of luminosity delivered by the LHC is taken from the CMS luminosity monitoring system [22]. For each luminosity section (a 23 s period defined by the trigger system) we multiply the luminosity in that section by the rate of detectable decays, to obtain a number of detectable decays produced within that section.

Next, the simulation determines when these decays take place. Each decaying particle is assigned a time of production that is spread equally amongst collision bunch-crossings and orbits within the luminosity section. A random lifetime is then drawn from an exponential distribution with time constant equal to the proper lifetime of the gluino, $\tau_{\tilde{g}}$. These two amounts of time are added to the time of the bunch-crossing within the orbit to determine the time at which

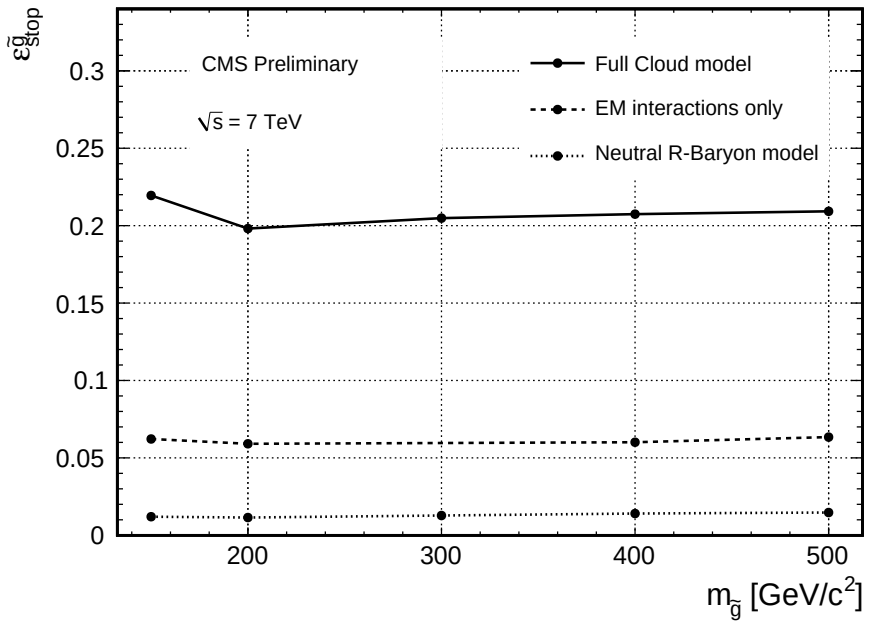

Figure 2: Probability, $\varepsilon^{\tilde{g}}_{stop}$, for a produced R-hadron to stop anywhere inside the CMS detector for different gluino masses, and $\sqrt{s} = 7$ TeV. The solid line shows the stopping efficiency for both electromagnetic and nuclear interactions, the dashed line shows that for electromagnetic interactions only, and the dotted line shows that for "neutral R-baryon" models in which only R-Mesons stop. For the purposes of this comparison, charge exchange reactions are considered NI.

the decay takes place.

The simulation performs similar steps to estimate the expected background. For this we use the rate of instrumental noise and cosmic-ray events, as measured during early 2010 collision data, described in Section 3. The background rate is multiplied by the trigger live-time and the resultant events are randomly assigned bunch-crossings and orbit numbers in either the collision or beam-gap periods.

Finally, the simulation determines whether each event takes place at a sensitive time and is "observable" or not. The number of observable events is recorded, and a counting experiment is performed, the results of which are presented in Section 5.

3 Event Selection

We run a dedicated trigger to search for decays of particles at times when there are no collisions. Information from the beam position and timing (BPTX) monitors are used to flag beam gaps. The BPTX monitors are positioned 175 m around the LHC ring either side of the CMS interaction region, and produce a signal when an LHC bunch passes the monitor. The coincidence of signals from both BPTX indicates bunches passing in both directions, and hence the possibility for a pp collision. For the stopped gluino search, we require a jet trigger together with the condition that a BPTX coincidence did not occur, ensuring that the trigger will not fire on jets produced from pp collisions. For the jet condition, we require a 10 GeV E_T threshold at the hardware trigger level (L1), and a 20 GeV energy threshold at the software trigger level

(HLT). At both L1 and HLT, we require the pseudorapidity of the jet, $|\eta_{jet}|$, to be less than 3.0.

We have used the simulation described in the previous sections to investigate the experimental signature of our atypical signal. Based on these studies, we have devised both topological and timing cuts which greatly reduce the instrumental and cosmic backgrounds while retaining good signal efficiency. These cuts are detailed in the rest of this section. As a benchmark for signal efficiency, we quote figures for the $m_{\tilde{g}} = 200\,\mathrm{GeV}/c^2$, $M_{\tilde{\chi}_1^0} = 100\,\mathrm{GeV}/c^2$ Monte Carlo sample.

In order to reject any background associated with an unpaired bunch passing through CMS, we veto any event in which a single BPTX has fired. Imperfections in the detector synchronisation may result in triggers from collisions events that are 1 bunch-crossing (BX) early or late with respect to the collision itself. We therefore reject any event falling within $\pm$ 1 BX of any passage of beam.

A small fraction of cosmic rays traversing CMS deposit significant energy in the calorimeters. To remove such background, we veto events which contain 1 or more muons.

Once beam related backgrounds and cosmic rays are removed, the remaining source of background is detector noise. We apply standard CMS calorimeter cleaning and noise rejection cuts [23–25]. In addition, we also make the following cuts on the shape and magnitude of hadronic calorimeter (HCAL) energy deposits in order to discriminate against HCAL instrumental noise.

Firstly, we restrict our search to jets in the central HCAL only. Since most gluino bound states are produced centrally due to their high mass, the endcaps and forward calorimeters (which tend to be noisier) do not contribute much to the signal rate. Hence we require that the most energetic jet in the event has $|\eta_{jet}| < 1.3$. In the subsequent selection described below, we refer to this jet.

To reject fluctuations over the jet threshold and energy deposits from minimum ionising particles we make a cut on the reconstructed jet energy at 50 GeV. To remove events where a single HCAL channel has fired, we veto events where the number of towers containing 90% of the energy (n_{90}) is 3 or less. We also veto wide jets characteristic of noise by removing events where the number of towers containing 60% of the leading jet energy (n_{60}) is less than 6. Noise may be distinguished from physical signals using the mapping of towers to their readout electronics. The 18 channels readout by a single hybrid photodiode all correspond to the same ϕ value, hence we order the HCAL towers by energy, and count the number of leading towers at the same ϕ. If this value, n_{iphi}, is greater than 5, we reject the event.

The HCAL electronics have a well-defined time response to charge deposits generated by showering particles. This pulse shape can be used to distinguish deposits from real physics processes from pulses generated by electronics noise, which may not have a physics-like time profile. A physical pulse has some notable properties which can be used to distinguish it from the noise pulses. There is a clear trigger-peak, (BX_{Peak}), significant energy in one bunch crossing before the peak (BX_{Peak-1}) and an exponential decay for several BX's following the peak. We have developed several powerful though correlated cuts that distinguish physical pulses from noise. We use the ratios $R_1 = BX_{peak+1}/BX_{peak}$ and $R_2 = BX_{peak+2}/BX_{peak+1}$ to characterize the exponential decay, requiring $0.15 < R_1$ and $0.10 < R_2 < 0.50$. Ten time samples (each 25 ns in length) are read out by the HCAL, allowing us to reject noise events based on the presence of energy in earliest or latest BX's, since the "physics pulse shape" covers only 4 time samples. We cut events with more than 10% of the energy of the pulse outside of the central four BX's. Deposits from physical particles tend to have a large fraction of the pulse energy in

the peak BX. Noise can have a variety of pulse shapes from having energy spread across many BX's to having almost all energy localized in one BX. We make a cut on the peak fraction of $0.4 < BX_{Peak}$ / Total Energy < 0.7.

The background rate and signal efficiency after each cut is summarized in Table 1. Table 2 shows the efficiencies for Monte Carlo samples with a range of $m_{\tilde{g}}$ and $M_{\tilde{\chi}_1^0}$. Note, that for parameter space points with sufficient visible energy, $m_{\tilde{g}} - M_{\tilde{\chi}_1^0} > 100$, the efficiency is approximately constant.

After all cuts, the efficiency for signal ($m_{\tilde{g}} = 200$ GeV and $M_{\tilde{\chi}_1^0} = 100$ GeV) estimated from the simulation, is 17.2% of all stopped particles, or 56.5% of all event passing the HLT. The final rate measured from the background sample, is $6.9 \pm 1.9(\text{stat}) \pm 2.1(\text{syst}) \times 10^{-5}$ Hz.

Table 1: Background rate determined from early 2010 collision data, and expected signal efficiency for the $m_{\tilde{g}} = 200$ GeV and $M_{\tilde{\chi}_1^0} = 100$ GeV Monte Carlo sample, after each online and offline cut. Note, the signal efficiency is quoted with respect to the fraction of events in which one of the two produced gluinos stops anywhere in the *whole* CMS detector.

Selection Criteria	Background Rate (Hz)	Signal Efficiency %
L1+HLT (HB+HE)	3.27	30.5
Calorimeter noise filters	1.12	29.9
BPTX/BX veto	1.11	29.9
muon veto	6.6×10^{-1}	26.4
$E_{jet} > 50$ GeV, $\lvert\eta_{jet}\rvert < 1.3$	7.6×10^{-2}	20.5
$n_{60} < 6$	7.6×10^{-2}	20.2
$n_{90} > 3$	3.1×10^{-3}	18.6
$n_{phi} < 5$	1.3×10^{-4}	18.5
$R_1 > 0.15$	1.1×10^{-4}	18.5
$0.1 < R_2 < 0.5$	8.5×10^{-5}	17.5
$0.4 < R_{peak} < 0.7$	7.9×10^{-5}	17.3
$R_{outer} < 0.1$	6.9×10^{-5}	17.2

Table 2: Selection efficiency as a function of $m_{\tilde{g}}$ and $M_{\tilde{\chi}_1^0}$

$m_{\tilde{g}}$ (GeV)	$M_{\tilde{\chi}_1^0}$ (GeV)	efficiency (% of stopped)
200	150	2.2%
300	250	3.0%
150	50	16.0%
200	100	17.2%
300	200	18.6%
400	300	18.7%
500	400	18.1%
300	100	19.4%
400	100	19.6%

4 Sources of Systematic Uncertainty

The generic search for stopped particles described in this note is, by design, minimally exposed to systematic uncertainties. As described in Section 1, the instrumental and cosmic ray background estimate applied to this search was obtained from data taken during beam-gaps of series of physics fills. We have restricted the search to certified good luminosity sections to ensure that these are identical conditions to that used for the search. Given these restrictions, the background rate is stable over many runs. However, independent monitoring of the HCAL noise shows the noise rate to fluctuate from one run to another. We use this independent measurement of the HCAL noise to estimate a systematic uncertainty of 30% on the background rate. There is a small systematic uncertainty due to the jet energy scale (JES). For a JES uncertainty of $\pm 10\%$, we estimate a 7% effect on the cross-section limit. The systematic uncertainty due to trigger efficiency is negligible since the data analysed are well above the turn-on region. Similarly, the systematic uncertainty due to reconstruction efficiency is negligible since we restrict our search to $m_{\tilde{g}} - M_{\tilde{\chi}_1^0} > 100$ GeV/c^2 wherein we are fully efficient. Finally, there is an 11% uncertainty on the luminosity.

Limits on a particular model (e.g. gluinos in split supersymmetry) introduce more substantial systematic uncertainties, since the signal yield is sensitive to the stopping probability. The GEANT4 simulation used to derive the stopping efficiency described in Section 2 implements models for both electromagnetic (EM) and nuclear interaction (NI) energy loss mechanisms. Whereas the EM model is well understood, the R-hadron "cloud model" used for NI has never been tested and is based on speculative physics extrapolated from low-energy QCD. Moreover, there are alternative models [21] in which R-hadrons preferentially become neutral after NI. While we think both the neutral R-hadron and EM only models are pessimistic scenarios, in Fig. 4 we present limits employing each of these models. The range spanned by these three curves represents the uncertainty on the limit due to the stopping model.

5 Results

After the selection criteria described in the preceding section are applied, we perform a counting experiment on the remaining data. We do this in bins of gluino lifetime from 75 ns to $\sim 10^7$ seconds. In addition to the bins required to map the general features of the exclusion limit, we include two lifetime bins for each observed event; the largest lifetime that excludes the event, and the smallest that includes it. For lifetime hypotheses shorter than one orbit, we search within a time-window following each filled bunch-crossing. The time window is optimised for sensitivity to that lifetime, of $1.256 \times \tau_{\tilde{g}}$. This restriction avoids the addition of backgrounds (which are constant in time) for time intervals during which the signal will have already decayed.

In the search sample, we do not see a significant excess above expected background in any lifetime bin. The results of this counting experiment for selected lifetime bins is presented in Table 3. In the absence of any discernible signal, we proceed to set 95% C.L. limits, using a Bayesian method, over 14 orders of magnitude in gluino lifetime. Figure 3 shows the 95% C.L. limit on $\sigma(pp \to \tilde{g}\tilde{g}) \times BR(\tilde{g} \to g\tilde{\chi}_1^0) \times \varepsilon_{stop}^{\tilde{g}\tilde{g}}$, where $\varepsilon_{stop}^{\tilde{g}\tilde{g}}$ is the probability for at least one of the two gluinos produced to stop. This is our experimental result; it is independent of models of R-hadron formation and subsequent nuclear interaction. In Fig. 4 we show the 95% C.L. limit on $\sigma(pp \to \tilde{g}\tilde{g}) \times BR(\tilde{g} \to g\tilde{\chi}_1^0)$ in which we employ the R-hadron models discussed above. Errors include statistical and systematic uncertainties. With the blue line in Fig. 4 we show a recent NLO+NLL calculation at $\sqrt{s} = 7$ TeV from the authors of [12]. The theoretical uncertainty

on this calculation (represented by the blue band) is taken to be 15%. To illustrate the effect of the stopping efficiency uncertainty, we show three different 95% C.L. limits on $\sigma(pp \rightarrow \tilde{g}\tilde{g}) \times BR(\tilde{g} \rightarrow g\tilde{\chi}_1^0)$ in which the different R-hadron models are used. For a mass difference $m_{\tilde{g}} - M_{\tilde{\chi}_1^0} > 100$ GeV, assuming BR($\tilde{g} \rightarrow g\tilde{\chi}_1^0$) = 100%, we are able to exclude lifetimes from 120 ns - 6 μs for $m_{\tilde{g}} = 200$ GeV/c^2 with the counting experiment. This result extends existing limits [26] which exclude lifetimes between 30 μs and 100 hours (indicated by the red line in Fig. 4).

Table 3: Results of counting experiments for selected $\tau_{\tilde{g}}$. Entries between 1e-3 and 1e+3 are identical to those of 1e-3 and 1e+3 and are suppressed.

Lifetime [s]	Expected Background ($\pm$ stat $\pm$ syst)	Observed
1e-07	$0.15 \pm 0.04 \pm 0.05$	0
1e-06	$1.8 \pm 0.5 \pm 0.5$	0
1e-05	$11.7 \pm 3.2 \pm 3.5$	8
1e-04	$28.3 \pm 7.8 \pm 8.5$	19
1e-03	$28.3 \pm 7.8 \pm 8.5$	19
1e+03	$28.3 \pm 7.8 \pm 8.5$	19
1e+04	$28.3 \pm 7.8 \pm 8.5$	19
1e+05	$28.3 \pm 7.8 \pm 8.5$	19
1e+06	$28.3 \pm 7.8 \pm 8.5$	19

Finally, we present the result as a function of the gluino mass in Fig. 5, for the lifetime bin in which the counting experiment is most sensitive, 2.6 μs. For a mass difference $m_{\tilde{g}} - M_{\tilde{\chi}_1^0} > 100$ GeV, assuming BR($\tilde{g} \rightarrow g\tilde{\chi}_1^0$) = 100%, we are able to exclude $m_{\tilde{g}} < 225$ GeV/c^2 for this lifetime.

6 Time Profile Results

In addition to the counting experiment performed in the preceding section, we also perform an analysis that involves the distribution of the observed events in time. A gluino signal is produced in a collision and eventually decays according to its lifetime, so the expected timing profile of gluino decays is strongly correlated with the timing profile of the delivered luminosity. On the other hand, the background contribution is not correlated with collisions and is flat in time. Since the signal and background contribution have very different time profiles, it is possible to extract them both by analysing the distribution of observed events in time.

We assume all colliding bunches in an orbit have equal individual instantaneous luminosity. Taking into account the relative integrated luminosities contributing to each of the filling schemes, we build an expected timing profile of gluino decays for a given gluino lifetime hypothesis. Figure 6 shows such a profile for a gluino lifetime of 1 μs together with flat background profile; the locations of observed events inside the orbit are overlaid. We limit the range of lifetime hypotheses considered for this time profile analysis to 75 ns - 100 μs since in order for the signal time structure to be clearly distinguishable from background, the gluino lifetime must be smaller than the orbit period, 89 μs. For each lifetime hypothesis we build a corresponding signal time profile, fit the signal plus background contribution to the data, and extract a 95% C.L. upper limit on the possible signal contribution. The obtained results are plotted as a dotted line in Fig. 4. This time analysis does not make use of a background prediction so has no corresponding systematic uncertainty. Consequently, its dominant systematic is the 11% on the luminosity. For a mass difference $m_{\tilde{g}} - M_{\tilde{\chi}_1^0} > 100$ GeV, assuming BR($\tilde{g} \rightarrow g\tilde{\chi}_1^0$)

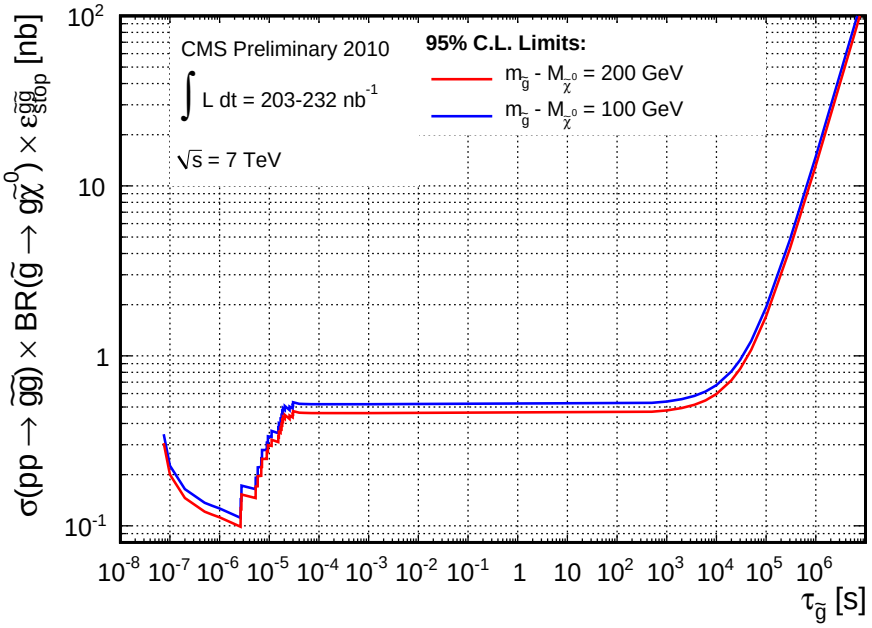

Figure 3: 95% C.L. limits on gluino pair production cross-section times the probability for at least one of the two gluinos produced to stop, as a function of gluino lifetime. Errors are statistical only. The structure observed between 10^{-6} s and 10^{-4} s is due to the number of observed events incrementing when crossing boundaries between lifetime bins. Also, see Fig. 6.

= 100%, we are able to exclude lifetimes from 75 ns - 3 μs for $m_{\tilde{g}} = 200$ GeV/c^2 with the time profile analysis. Finally, we present the result of the time profile analysis as a function of the gluino mass in Fig. 5. For a mass difference $m_{\tilde{g}} - M_{\tilde{\chi}_1^0} > 100$ GeV, assuming BR($\tilde{g} \rightarrow g\tilde{\chi}_1^0$) = 100%, we are able to exclude $m_{\tilde{g}} < 229$ GeV/c^2 for a lifetime of 200 ns with the time profile analysis.

7 Conclusions

In this PAS we have presented the first results of a search for long-lived gluinos which have stopped in the CMS detector after being produced in 7 TeV pp collisions from CERN's LHC. We looked for the subsequent decay of these particles during time intervals where there were no pp collisions in the CMS experiment. In particular, we searched for decays during gaps between crossings in the LHC beam structure. We recorded such decays with dedicated calorimeter triggers. In a dataset with a peak instantaneous luminosity of 1.3×10^{30}cm^{-2}s^{-1}, an integrated luminosity of 203 - 232 nb^{-1} depending on the gluino lifetime, and a search interval corresponding to 115 hours of LHC operation, no significant excess above background was observed. In the absence of a signal, we set a limit at 95% C.L. on gluino pair production over 14 orders of magnitude of gluino lifetime. For a mass difference $m_{\tilde{g}} - M_{\tilde{\chi}_1^0} > 100$ GeV, assuming BR($\tilde{g} \rightarrow g\tilde{\chi}_1^0$) = 100%, we are able to exclude lifetimes from 75 ns - 6 μs for $m_{\tilde{g}} = 200$ GeV/c^2. This result extends existing limits from the Tevatron which exclude lifetimes between 30 μs and 100 hours [26]. Furthermore we exclude gluino masses $m_{\tilde{g}} < 229$ GeV/c^2 with a lifetime of 200 ns using a time-profile analysis and $m_{\tilde{g}} < 225$ GeV/c^2 with a lifetime of 2.6 μs in a counting experiment. This result is consistent with the complementary exclusion provided by our direct HSCP search [27]. As more luminosity is delivered by the LHC the reach of this analysis will

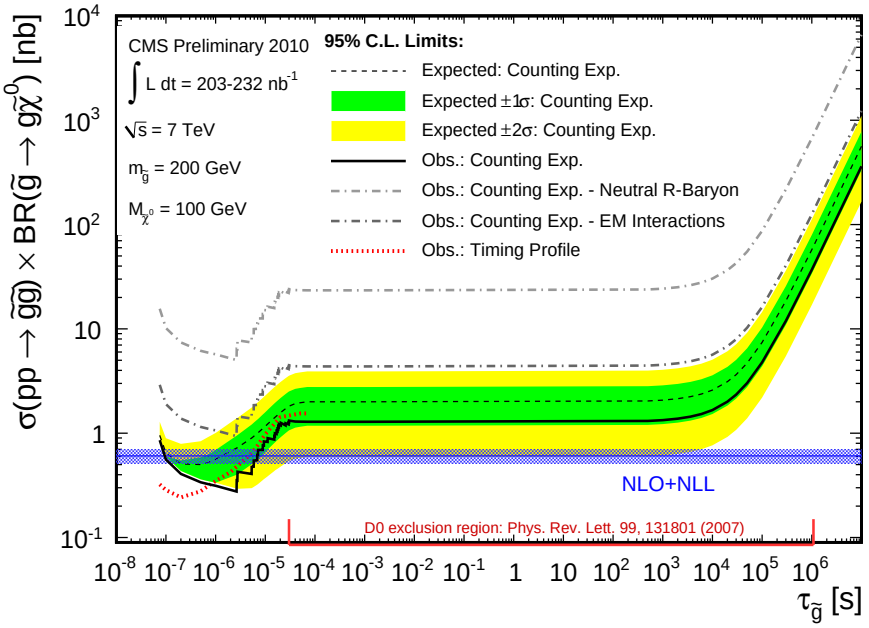

Figure 4: Expected and observed 95% C.L. limits on gluino pair production cross-section using the "cloud model" of R-hadron interactions as a function of gluino lifetime from both counting experiment and the time profile analysis. Errors include statistical plus systematic uncertainties. Observed 95% C.L. limits on the gluino cross-section for alternative R-hadron interaction models are also presented. The NLO+NLL calculation is from a private communication with the authors of [12]. The theoretical uncertainty on this calculation (represented by the blue band) is taken to be 15%. The lifetime range excluded by D0 in [26] is indicated by the red line. The structure observed between 10^{-6} s and 10^{-4} s is due to the number of observed events incrementing when crossing boundaries between lifetime bins. Also, see Fig. 6.

improve rapidly. In particular, since the only backgrounds to this search are independent of luminosity, this sensitivity will increase significantly when the LHC peak instantaneous luminosity increases to 10^{32} cm^{-2}s^{-1} expected later this year.

References

[1] M. Fairbairn et al., "Stable massive particles at colliders", *Phys. Rept.* **438** (2007) 1–63, arXiv:hep-ph/0611040. doi:10.1016/j.physrep.2006.10.002.

[2] S. Dimopoulos, M. Dine, S. Raby et al., "Experimental Signatures of Low Energy Gauge Mediated Supersymmetry Breaking", *Phys. Rev. Lett.* **76** (1996) 3494–3497, arXiv:hep-ph/9601367. doi:10.1103/PhysRevLett.76.3494.

[3] H. Baer, K.-m. Cheung, and J. F. Gunion, "A Heavy gluino as the lightest supersymmetric particle", *Phys. Rev.* **D59** (1999) 075002, arXiv:hep-ph/9806361. doi:10.1103/PhysRevD.59.075002.

[4] T. Jittoh, J. Sato, T. Shimomura et al., "Long life stau", *Phys. Rev.* **D73** (2006) 055009, arXiv:hep-ph/0512197. doi:10.1103/PhysRevD.73.055009.

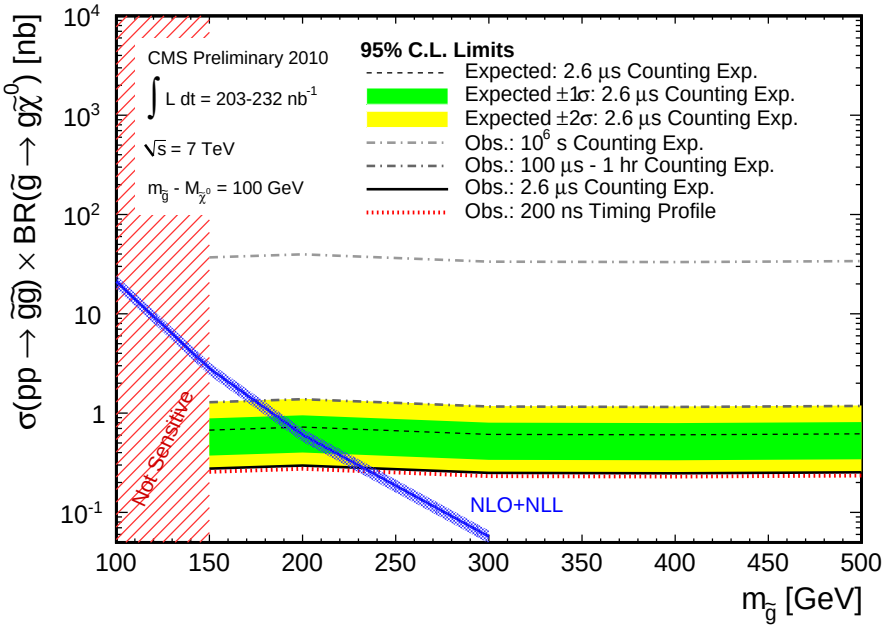

Figure 5: 95% C.L. limits on gluino pair production cross-section as a function of gluino mass assuming the "cloud model" of R-hadron interactions. The $m_{\tilde{g}} - M_{\tilde{\chi}_1^0}$ mass difference is maintained at 100 GeV; results are only presented for $M_{\tilde{\chi}_1^0} > 50$ GeV. The NLO+NLL calculation is from a private communication with the authors of [12]. The theoretical uncertainty on this calculation (represented by the blue band) is taken to be 15%. The lifetimes chosen are those for which the counting experiment and time profile analysis are most sensitive. With the counting experiment, we exclude $m_{\tilde{g}} < 225$ GeV/c^2 for a lifetime of 2.6 μs, and with the time profile analysis we exclude $m_{\tilde{g}} < 229$ GeV/c^2 for a lifetime of 200 ns.

[5] M. J. Strassler and K. M. Zurek, "Echoes of a hidden valley at hadron colliders", *Phys. Lett.* **B651** (2007) 374–379, arXiv:hep-ph/0604261. doi:10.1016/j.physletb.2007.06.055.

[6] M. J. Strassler, "Possible effects of a hidden valley on supersymmetric phenomenology", arXiv:hep-ph/0607160.

[7] A. Arvanitaki et al., "Astrophysical Probes of Unification", *Phys. Rev.* **D79** (2009) 105022, arXiv:0812.2075. doi:10.1103/PhysRevD.79.105022.

[8] N. Arkani-Hamed and S. Dimopoulos, "Supersymmetric unification without low energy supersymmetry and signatures for fine-tuning at the LHC", *JHEP* **06** (2005) 073, arXiv:hep-th/0405159.

[9] S. Dawson, E. Eichten, and C. Quigg, "Search for Supersymmetric Particles in Hadron - Hadron Collisions", *Phys. Rev.* **D31** (1985) 1581. doi:10.1103/PhysRevD.31.1581.

[10] W. Beenakker, R. Hopker, M. Spira et al., "Squark and gluino production at hadron colliders", *Nucl. Phys.* **B492** (1997) 51–103, arXiv:hep-ph/9610490. doi:10.1016/S0550-3213(97)00084-9.

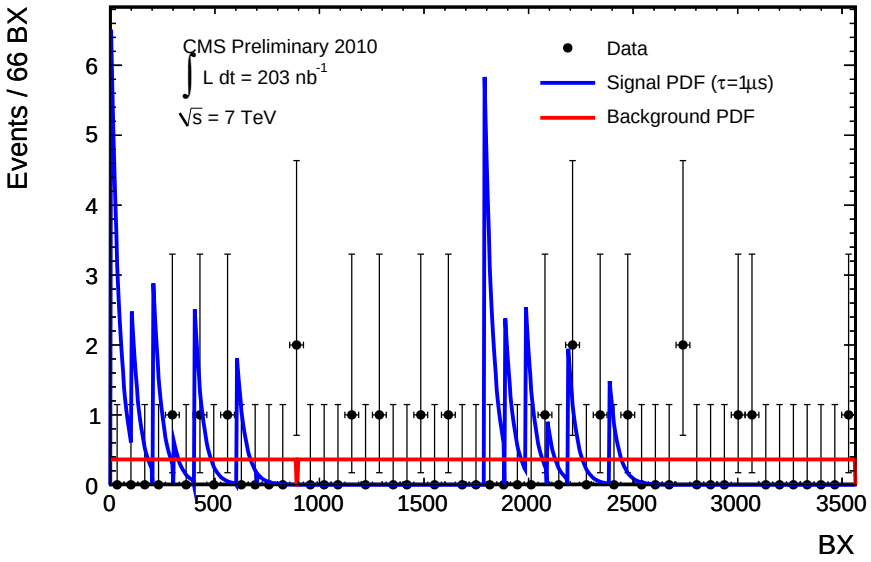

Figure 6: The in-orbit position of the 19 observed events is overlaid on top of the decay profile for a 1 μs lifetime hypothesis and a flat background. The spikes in the signal profile correspond to the weighted contributions from collisions in the following BX: 1, 101, 201, 301, 401, 601, 1786, 1886, 1986, 2086, 2186, 2386, which are filled with proton bunches in the different 2×2, 3×3, 4×4, 6×6, and 8×8 LHC beam structures used in this analysis.

[11] T. Plehn, D. Rainwater, and P. Z. Skands, "Squark and gluino production with jets", *Phys. Lett.* **B645** (2007) 217–221, arXiv:hep-ph/0510144. doi:10.1016/j.physletb.2006.12.009.

[12] W. Beenakker et al., "Soft-gluon resummation for squark and gluino hadroproduction", *JHEP* **12** (2009) 041, arXiv:0909.4418. doi:10.1088/1126-6708/2009/12/041.

[13] A. Arvanitaki, C. Davis, P. W. Graham et al., "Limits on split supersymmetry from gluino cosmology", *Phys. Rev.* **D72** (2005) 075011, arXiv:hep-ph/0504210. doi:10.1103/PhysRevD.72.075011.

[14] T. Jittoh et al., "Stau properties from the Big-Bang Nucleosynthesis and the relic abundance of dark matter", *Phys. Rev.* **D78** (2008) 055007, arXiv:0805.3389. doi:10.1103/PhysRevD.78.055007.

[15] A. Arvanitaki, S. Dimopoulos, A. Pierce et al., "Stopping gluinos", *Phys. Rev.* **D76** (2007) 055007, arXiv:hep-ph/0506242. doi:10.1103/PhysRevD.76.055007.

[16] CMS Collaboration, "Search for Heavy Stable Charged Particles with 100 pb^{-1} and 1 fb^{-1} in the CMS experiment", *CMS-PAS* **EXO-08-003** (2008).

[17] CMS Collaboration, "Searching for Stopped Gluinos during Beam-off Periods at CMS", *CMS-PAS* **EXO-09-001** (2009).

[18] T. Sjostrand, S. Mrenna, and P. Z. Skands, "PYTHIA 6.4 Physics and Manual", *JHEP* **05** (2006) 026, arXiv:hep-ph/0603175.

[19] GEANT4 Collaboration, "GEANT4: A simulation toolkit", *Nucl. Instrum. Meth.* **A506** (2003) 250–303. doi:10.1016/S0168-9002(03)01368-8.

[20] R. Mackeprang and A. Rizzi, "Interactions of coloured heavy stable particles in matter", *Eur. Phys. J.* **C50** (2007) 353–362, arXiv:hep-ph/0612161. doi:10.1140/epjc/s10052-007-0252-4.

[21] F. Buccella, G. R. Farrar, and A. Pugliese, "R BARYON MASSES", *Phys. Lett.* **B153** (1985) 311. doi:10.1016/0370-2693(85)90555-6.

[22] CMS Collaboration, "Measurement of CMS Luminosity", *CMS-PAS* **EWK-10-004** (2010).

[23] CMS Collaboration, "Identification and Filtering of Uncharacteristic Noise in the CMS Hadron Calorimeter", *JINST* **5** (2010) T03014, arXiv:0911.4881. doi:10.1088/1748-0221/5/03/T03014.

[24] CMS Collaboration, "HCAL Commissioning in Proton Collisions at $\sqrt{s} = 7$ TeV", *CMS-PAS* **JME-10-007** (2010).

[25] CMS Collaboration, "MET Performance in Minimum-Bias and Jet Events from Proton-Proton Collisions at $\sqrt{s} = 7$ TeV", *CMS-PAS* **JME-10-004** (2010).

[26] D0 Collaboration, "Search for stopped gluinos from $p\bar{p}$ collisions at $\sqrt{s}$ = 1.96-TeV", *Phys. Rev. Lett.* **99** (2007) 131801, arXiv:0705.0306. doi:10.1103/PhysRevLett.99.131801.

[27] CMS Collaboration, "Search for Heavy Stable Charged Particles in pp collisions at $\sqrt{s} = 7$ TeV", *CMS-PAS* **EXO-10-004** (2010).